Inorganic Chemistry

Article

pubs.acs.org/IC

A Three-Pronged Attack To Investigate the Electronic Structure of a Family of Ferromagnetic Fe_4Ln_2 Cyclic Coordination Clusters: A Combined Magnetic Susceptibility, High-Field/High-Frequency Electron Paramagnetic Resonance, and ^{57}Fe Mössbauer Study

Sebastian F. M. Schmidt,[†] Changhyun Koo,[‡] Valeriu Mereacre,[†] Jaena Park,[‡] Dieter W. Heermann,[§] Vladislav Kataev,[∥] Christopher E. Anson,[†] Denis Prodius,[⊥] Ghenadie Novitchi,[#] Rüdiger Klingeler,*[,‡,▽] and Annie K. Powell*[,†,○]

[†]Institut für Anorganische Chemie, Karlsruher Institut für Technologie, Engesserstrasse 15, 76131 Karlsruhe, Germany

[‡]Kirchhoff Institute of Physics and [▽]Centre for Advanced Materials (CAM), Im Neuenheimer Feld 227, Heidelberg University, 69120 Heidelberg, Germany

[§]Institute for Theoretical Physics, Philosophenweg 16, Heidelberg University, 69120 Heidelberg, Germany

[∥]Leibniz Institute for Solid State and Materials Research, Helmholtzstrasse 20, IFW Dresden, 01069 Dresden, Germany

[⊥]Institute of Chemistry, Academy of Sciences of Moldova, Chisinau, Moldova

[#]Laboratoire National des Champs Magnétiques Intenses, UPR CNRS 3228, Grenoble, France

[○]Karlsruhe Institute of Technology, Institute of Nanotechnology, Herrmann-von-Helmholtz-Platz 1, 76344 Eggenstein-Leopoldshafen, Germany

Supporting Information

ABSTRACT: We present the synthesis, structure, magnetic properties, as well as the Mössbauer and electron paramagnetic resonance studies of a ring-shaped $[Fe^{III}_4Ln^{III}_2(Htea)_4(\mu\text{-}N_3)_4(N_3)_3(piv)_3]$ (Ln = Y **1**, Gd **2**, Tb **3**, Dy **4**, Ho **5**, Er, **6**) coordination cluster. The Dy, Tb, and Ho analogues show blocking of the magnetization at low temperatures without applied fields. The anisotropy of the 3d ion and the exchange interaction between 3d and 4f ions in Fe_4Ln_2 complexes are unambiguously determined by high-field/high-frequency electron paramagnetic resonance measurements at low temperature. Ferromagnetic exchange interaction J_{Fe-Ln} is found which decreases upon variation of the Ln ions to larger atomic numbers. This dependence is similar to the behavior shown in the effective barrier values of complexes **3**−**5**. Further information about the anisotropy of the Ln^{3+} ions was gathered with ^{57}Fe Mössbauer spectroscopy, and the combination of these methods provides detailed information regarding the electronic structure of these complexes.

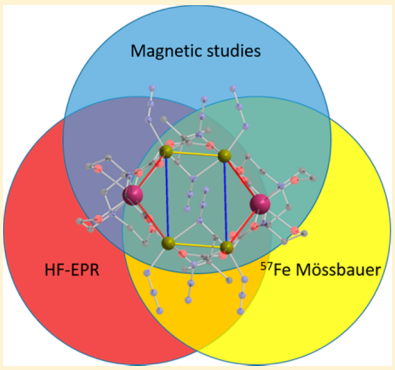

INTRODUCTION

Single molecule magnets (SMM) are coordination clusters that show behavior similar to bulk ferro- or ferrimagnets due to the blocking of magnetization below a given temperature. The fact that the origin of their magnetic properties is quantum mechanical means that they are candidates for higher density data storage and quantum computing.[1−3] While the first examples of such molecular magnets contain mostly 3d metals such as manganese,[4−7] the discovery of lanthanide (Ln)-based SMMs[8] where the anisotropy of the Ln ion causes the SMM behavior opens the door to a new and fascinating area of coordination cluster chemistry. Because of the lanthanides' unquenched orbital momentum, higher energy barriers against the reversal of magnetization can be achieved, but it was only recently possible to surpass the blocking temperature of transition metal-based SMMs.[9−13] This discrepancy is caused by tunneling and spin-phonon based relaxation pathways, that are less pronounced in 3d SMMs, so that it is often impossible to obtain open hysteresis loops or even slow magnetic relaxation without application of a *dc* field.[14−16] Although combining the anisotropy of 4f metals with the slow relaxation rate of exchange coupled 3d systems sounds like a logical step, there are only a few examples where a paramagnetic 3d ion is able to slow down the relaxation speed.[17] Additionally the magnetic exchange interaction between a 3d metal and a strongly spin orbit coupled 4f metal in an SMM leads to challenging problems in determining the electronic structure. In order to understand the magnetic properties, it is necessary to perform extra methods such as quantum chemical calculations[13,17−23] or further spectroscopic methods.[7,24−32]

Received: November 8, 2016
Published: February 10, 2017

DOI: 10.1021/acs.inorgchem.6b02682
Inorg. Chem. 2017, 56, 4796−4806

We recently published the coordination clusters $[Fe^{III}_4Ln^{III}_2(Htea)_4(\mu\text{-}N_3)_4(piv)_6]$ (Ln Er, Lu; $teaH_3$ = triethanolamine and piv = pivalate anion), which are the first Fe/Ln clusters to show ferromagnetic interactions between two irons as well as between the Fe^{III} and the Ln^{III}.[32] We now report six other complexes closely isostructural to these two, with lighter lanthanides or the rare earth cation Y, $[Fe^{III}_4Ln^{III}_2(Htea)_4(\mu_2\text{-}N_3)_4(N_3)_3(piv)_3]$ (Ln = Y **1**, Gd **2**, Tb **3**, Dy **4**, Ho **5**, Er **6**), which crystallize as an isotypic series. We present a systematic and comparative study of the magnetic behavior of **1**−**6**, using a combination of magnetic susceptibility measurements, variable-field ^{57}Fe Mössbauer spectroscopy, and high-field/high-frequency electron paramagnetic resonance (HF-EPR) studies to probe the magnetic interactions and anisotropy within this family of complexes. The combination of these techniques allows the correlation of different measurement frequencies with the exchange interactions in the molecule.

EXPERIMENTAL SECTION

General Procedures. Unless otherwise stated, all reagents were obtained from commercial sources and were used as received without further purification. The synthesis of complex **6** has been previously described.[32] All reactions were carried out under aerobic conditions. Elemental analyses (CHN) were performed using an Elementar Vario EL analyzer. Fourier transform infrared spectra were measured as KBr pellets over 4000−400 cm^{-1} on a PerkinElmer *Spectrum One* spectrometer. *Caution! Although no such tendency was observed during the present work, azide salts are potentially explosive and should be handled with care and in small quantities.*

Syntheses of Complexes. *$[Fe_3O(piv)_6(H_2O)_3](piv)\cdot 2pivH$.* A mixture of $Fe(NO_3)_3\cdot 9H_2O$ (10.0 g, 24.8 mmol) and pivalic acid (28.0 g, 274.0 mmol) were heated for 2 h at 200 °C until there was no more gas formation. After the mixture was cooled under 100 °C, a mixture of 85 mL of ethanol and 15 mL of water were added. Overnight red brown hexagon-shaped crystals appeared. Calc for $[Fe_3O(piv)_6(H_2O)_3](piv)\cdot 2pivH$ C, 44.46; H, 7.36; N, 0.00%. Found: C, 45.10; H, 7.745; N, 0.00%.

$[Fe_4Gd_2(teaH)_4(N_3)_{7.32}(piv)_{2.68}]\cdot 4H_2O$ **2**. The ligand $teaH_3$ (= triethanolamine) (425 mg, 2.85 mmol), $[Fe^{III}_3O(Piv)_6(H_2O)_3]\cdot Piv\cdot 2PivH$ (250 mg, 0.24 mmol), $Fe(NO_3)_3\cdot 9H_2O$ (300 mg, 0.74 mmol), sodium azide (290 mg, 4.46 mmol), and $Gd(NO_3)_3\cdot 6H_2O$ (343 mg, 0.74 mmol) was dissolved under constant stirring in 20 mL of ethanol, and the solution was heated for 30 min to boiling. After that the solution was filtered, and the filtrate was left in a closed vial under ambient conditions. After 1 h orange crystals suitable for single crystal crystallography formed in a good yield. Although the use of two different Fe^{III} sources is unusual, the use of only $[Fe^{III}_3O(Piv_6(H_2O)_3][Piv]$ or a combination of $Fe(NO_3)_3\cdot 9H_2O$ and pivalic acid will result in the formation of $[Fe^{III}_8(\mu_4O)_3(\mu_4\text{-tea})(teaH)_3(O_2CCMe_3)_6(N_3)_3]$.[55]

Calc for $[Fe_4Gd_2(teaH)_4(N_3)_{7.32}(piv)_{2.68}]\cdot 4H_2O$ **1**: C 25.28, H 4.77, N 20.46; found C 25.18, H 4.75, N 20.40. IR (KBr) /cm^{-1}: 3421 (b, m), 2963 (m), 2904 (m), 2860 (s), 2099 (s), 2078 (s), 2060 (s), 1539 (s), 1484 (m), 1459 (w), 1423 (m), 1365 (b, w), 1285 (w), 1228 (m), 1095 (s), 1073 (s), 1024 (m), 920 (m), 901 (s), 649 (m), 608 (m), 553 (w), 490 (m).

$[Fe_4Tb_2(teaH)_4(N_3)_7(piv)_3]\cdot 3H_2O$ **3**. Compound **3** was synthesized in a similar way with the appropriate $Tb(NO_3)_3\cdot 6H_2O$. Calc for $[Fe_4Tb_2(teaH)_4(N_3)_7(piv)_3]\cdot 3H_2O$ **2**: C 26.12, H 4.78, N 19.52; found C 26.05, H 4.76, N 19.70. IR (KBr) /cm-1:3410 (b, m), 2962 (m), 2900 (m), 2863 (s), 2099 (s), 2077 (s), 2059 (s), 1539 (s), 1484 (m), 1458 (w), 1423 (s), 1365 (w), 1353 (w), 1285 (w), 1229 (m), 1094 (s), 1072 (s), 1023 (m), 919 (m), 900 (s), 648 (m), 608 (m), 551 (w), 488 (m).

$[Fe_4Dy_2(teaH)_4(N_3)_7(piv)_3]\cdot 3.5H_2O\cdot 1/2EtOH$ **4**. Compound **4** was synthesized in a similar way with $Dy(NO_3)_3\cdot 6H_2O$. Calc for $[Fe_4Dy_2(teaH)_4(N_3)_7(piv)_3]\cdot 3\text{-}1/2H_2O\cdot 1/2EtOH$ **3**: C 26.39, H 4.93, N 19.23; found C 26.39, H 4.80, N 19.27. IR (KBr) /cm-1:3393 (b, m), 2962 (m), 2900 (m), 2864 (s), 2095 (s), 2077 (s), 2061 (s), 1540 (s), 1484 (m), 1458 (w), 1423 (s), 1385 (w), 1364 (w), 1285 (w), 1228 (m), 1095 (s), 1074 (s), 1023 (m), 916 (m), 900 (s), 647 (m), 608 (m), 555 (w), 489 (w).

$[Fe_4Ho_2(teaH)_4(N_3)_7(piv)_3]\cdot 3.3H_2O\cdot 0.7EtOH$ **5**. Compound **5** was synthesized in a similar way with $Ho(NO_3)_3\cdot 6H_2O$. Calc for $[Fe_4Ho_2(teaH)_4(N_3)_7(piv)_3]\cdot 3.3H_2O\cdot 0.7EtOH$ **4**: C 26.50, H 4.94, N 19.12; found C 26.53, H 4.78, N 19.20. IR (KBr) /cm^{-1}: 3402 (b, m), 2963 (m), 2900 (m), 2864 (s), 2100 (s), 2079 (s), 2054 (s), 1536 (s), 1484 (m), 1458 (w), 1423 (s), 1366 (w), 1353 (w), 1285 (w), 1229 (m), 1094 (s), 1072 (s), 1023 (m), 919 (m), 900 (s), 648 (m), 608 (m), 551 (w), 488 (m).

$[Fe_4Er_2(teaH)_4(N_3)_7(piv)_3]\cdot 2.5H_2O$ **6**. Compound **6** was synthesized in a similar way with $Er(NO_3)_3\cdot 6H_2O$. Calc for $[Fe_4Er_2(teaH)_4(N_3)_7(piv)_3]\cdot 2\text{-}1/2H_2O$: C 26.64, H 4.81, N 19.91; found C 26.63, H 4.81, N 19.84. IR (KBr) /cm^{-1}: 3407 (b, m), 2957 (m), 2898 (m), 2858 (s), 2099 (s), 2075 (s), 2056 (s), 1536 (s), 1480 (m), 1454 (w), 1421 (m), 1361 (w), 1348 (w), 1282 (w), 1230 (m), 1092 (s), 1069 (s), 1020 (m), 918 (m), 898 (s), 645 (m), 605 (m), 546 (w), 480 (m).

$[Fe_4Y_2(teaH)_4(N_3)_7(piv)_3]\cdot 4H_2O\cdot 0.5EtOH$ **1**. Compound **1** was synthesized in a similar way with $Y(NO_3)_3\cdot 6H_2O$. Calc for $[Fe_4Y_2(teaH)_4(N_3)_7(piv)_3]\cdot 4H_2O\cdot 1/2EtOH$ **5**: C 28.55, H 5.39, N 20.81; found C 28.50, H 5.13, N 20.76. IR (KBr) /cm^{-1}: 3404 (b, m), 2955 (m), 2896 (m), 2856 (s), 2096 (s), 2077 (s), 2058 (s), 1537(s), 1480 (m), 1454 (w), 1423 (m), 1360 (w), 1346 (w), 1280 (w), 1231 (m), 1094 (s), 1067 (s), 1026 (m), 916 (m), 898 (s), 649 (m), 609 (m), 540 (w), 482 (m).

X-ray Crystallography. Data were measured at 100 K on a Bruker SMART Apex diffractometer (**2**, **3**) or at 150 K on a Stoe IPDS II diffractometer (**1**, **4**, **5**) with graphite-monochromated Mo−Kα radiation. Structure solution was by direct methods, and full-matrix least-squares refinement was carried out using SHELXL-2014.[33−35] Ordered non-H atoms were refined with anisotropic temperature factors, while disordered groups were refined with combinations of partial occupancy isotropic atoms, with geometric similarity restraints as appropriate. Organic H atoms were placed in idealized positions; the coordinates of H atoms bonded to oxygen were refined with restrained O−H distances. The Fe_4Y_2 complex **1** invariably forms rather smaller crystals than the other compounds, and the data set used here only had significant diffraction to 0.95 Å resolution (2θ = 46.5°); however, the structure was completely adequate to show that **5** was isostructural to the other analogues.

Numerical details of the structures and refinements are given in Table S3. Crystallographic data (excluding structure factors) for the structures in this paper have been deposited with the Cambridge Crystallographic Data Centre as supplementary publication nos. CCDC 1453495−1453499. Copies of the data can be obtained, free of charge, on application to CCDC, 12 Union Road, Cambridge CB2 1EZ, UK: https://summary.ccdc.cam.ac.uk/structure-summary-form, or fax: + 44 1223 336033.

Magnetic Measurements. Magnetic susceptibility data (2−300 K) were collected on powdered polycrystalline samples on a Quantum Design MPMS-XL SQUID magnetometer under an applied magnetic field of 0.1 T. *ac* measurements were performed in the 2−10 K range using a 3.0 Oe *ac* field oscillation in 1−1500 Hz range. Magnetization isotherms were collected at 2 K between 0 and 5 T. All samples were constrained in eicosane. All data were corrected from the sample holder contribution and the diamagnetism of the samples estimated from Pascal's constants.[36,37] Magnetic data analyses were carried out by calculations of energy levels associated with the spin Hamiltonians presented in the text, and with the MAGPACK program package.[38]

HF-EPR Data. High-frequency electron paramagnetic resonance (HF-EPR) measurements were carried out on compounds **1**−**5** over the frequency range 80−600 GHz, and between 4 and 30 K. In this setup a millimeter vector network analyzer (MVNA) is used as both the source and detector of frequency-stabilized microwaves. A superconducting magnet provides magnetic fields of up to 16 T.[39] Powder samples were not restrained enabling self-alignment of the powder particles under application of a strong magnetic field. In order to investigate the frequency dependence of EPR spectra of the

DOI: 10.1021/acs.inorgchem.6b02682
Inorg. Chem. 2017, 56, 4796−4806

complexes, HF-EPR measurements were performed on all compounds at 4 K at various frequencies. The temperature dependence of the resonance peaks was investigated at a fixed frequency upon variation of temperature from 4 to 30 K.

Mössbauer Spectroscopy. Variable temperature Mössbauer spectra both with and without applied field were recorded using a conventional spectrometer in constant−acceleration mode equipped with a ^{57}Co source (3.7 GBq) in rhodium matrix. Isomer shifts are given relative to α-Fe at 300 K.

RESULTS AND DISCUSSION

Syntheses and Molecular Structures. The syntheses of the previously published Fe_4Er_2 and Fe_4Lu_2 compounds[32] were optimized in order to obtain lighter lanthanide analogues and to increase the yield. This however leads to complexes in which the monodentate ligands coordinated to Fe(1) and Fe(1′) are a disordered mixture of azide and pivalate for compounds **1**−**5**; the relative amounts of these found from the crystal structures was consistent with microanalytical data. Reaction of $[Fe^{III}_3O(Piv)_6(H_2O)_3](Piv)\cdot 2HPiv$, $Ln(NO_3)_3\cdot 6H_2O$, $Fe(NO_3)_3\cdot 6H_2O$, $teaH_3$, and NaN_3 (1:3:3:12:18) in ethanol yields a red solution from which orange crystals are obtained after several hours.

Complexes **1**−**5** crystallize isotypically in the monoclinic space group $P2_1/n$ with $Z = 2$. The structure of the Fe_4Dy_2 complex **4** will be described here in detail (Figure 1); all the others are isostructural. The structure of **4** is based on a centrosymmetric cyclic Fe_4Dy_2 core, in which the six metal cations are all coplanar to within 0.0125(5) Å. It can usefully be considered as being made up from two $\{Fe_2(\mu\text{-}N_3)_2(\mu\text{-}piv)(L)_2\}^+$ and two $\{Dy(teaH)_2\}^-$ building blocks. Each Dy^{III} cation is chelated by two doubly deprotonated $(teaH)^{2-}$, resulting in an octacoordinate (N_2O_6) distorted dodecahedral coordination environment. One deprotonated oxygen from each of these $(teaH)^{2-}$ ligand on a Dy center coordinates to a Fe of one of the dinuclear units, so that each Dy··Fe linkage in the ring involves a pair of alkoxo bridges. These four linkages are all very similar in terms of geometry, with Dy−O 2.288(4)−2.389(5) Å, Fe−O 1.941(4)−1.958(5) Å and the Dy−O−Fe angles 105.42(18)−105.92(19)°.

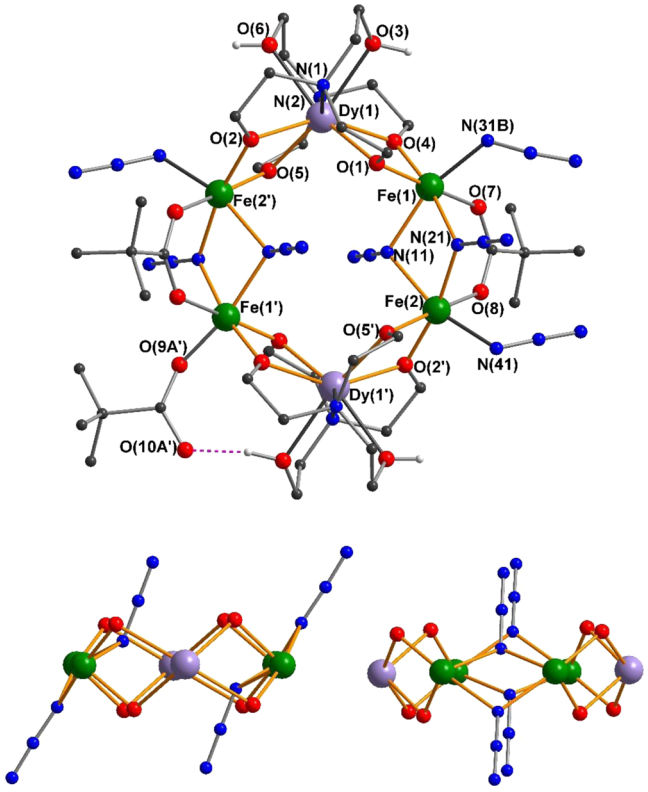

Figure 1. Molecular structure of **4** (above); two views of the core of **4** emphasizing the planarity of the Fe_4Dy_2 ring (below). Organic H atoms omitted for clarity; only one of the possible combinations of disordered pivalate and azide on Fe(1) and Fe(1′) is shown. Primed atoms result from the symmetry operation $-x + 1, -y + 1, -z + 1$.

Within the dinuclear Fe_2 moieties, the two Fe^{III} cations are bridged by a pair of end-on (μ-N_3) ligands and a syn,syn-bridging pivalate. The two azide bridges are both similar and symmetrical, with Fe−N 2.101(6)−2.142(6) Å and Fe−N−Fe 99.7(2) and 102.0(2)°. The Fe··Fe distance within the unit is 3.2683(7) Å. The dihedral angle between the Fe_2N_2 mean plane and the plane of the Fe_4Dy_2 ring is 44.8°. The distorted octahedral coordination environment on Fe(2) is completed by a terminal azide ligand. On Fe(1), the last site is filled by a disordered superposition of an azide and a monodentate pivalate. As a consequence of the relatively short intermolecular distance between Fe(1) and its equivalent at $-x + 1, -y, -z + 1$, it is not possible for the terminal ligands on both these irons to be pivalate, as unrealistically short contacts would result if one of these ligands is pivalate the other is azide. Indeed, for compounds **1** and **3**−**5**, each molecule has on average three terminal azides and one pivalate, as shown by both the structural refinements and the microanalytical data. For the Fe_4Gd_2 compound **2**, the average composition was slightly more in favor of azide, with 3.32 azides and 0.68 pivalates giving the best fit to the CHN data and also giving more similar thermal parameters for O(9A) and N(31B) in the crystal structure. This disorder was not found in the procedure published before in which the compound was recrystallized in acetonitrile with a drawback of a drastically reduced yield.[32] Within the crystal structure, there are no intercluster pathways mediated by hydrogen-bonding or other supramolecular interactions.

Magnetic Properties. In order to evaluate the nature of magnetic interactions between the Fe^{III}−Fe^{III} and Fe^{III}−Ln^{III} ions in Fe_4Ln_2 series as well the presence of interaction through the diamagnetic Y^{III} ion the compounds **1**−**5** have been magnetically characterized. The magnetic susceptibilities of **1**−**5** have been measured over the temperature range 1.8−300 K under an applied field of 0.1 T (see Figures 2, 3, SI5, SI6 and numerical data in Table 1). The χT product of Fe_4Y_2 (**1**) has a room temperature value of 19.31 cm^3 mol^{-1} K which is slightly higher than the theoretical expected value for four uncoupled Fe^{III} ions (d^5, $S = 5/2$, $g = 2$) 17.514 cm^3 mol^{-1} K. With decreasing temperature the χT product rises steadily to a maximal value of 26.02 cm^3 mol^{-1} K at 25.0 K. From there it drops to a value of 10.74 cm^3 mol^{-1} K at 2 K. This behavior suggests the presence of a predominant ferromagnetic interactions in **1**. Low temperature decreasing of χT product can be related to existence of weaker antiferromagnetic interactions between the two different $\{Fe_2\}$ units in the molecule,[40] zero field splitting (ZFS) of Fe^{III}, as well as presence of intermolecular interactions between neighboring Fe_4Y_2 clusters.

Complex **2** (Fe_4Gd_2) at room temperature has a magnetic susceptibility value equal to 35.07 cm^3 mol^{-1} K which is close to the theoretical value of 33.25 cm^3 mol^{-1} K (four Fe^{III} d^5, $S = 5/2$, $g = 2$ and two Gd^{III} f^7 $g = 2$, $S = 7/2$). The maximum value

DOI: 10.1021/acs.inorgchem.6b02682
Inorg. Chem. 2017, 56, 4796−4806

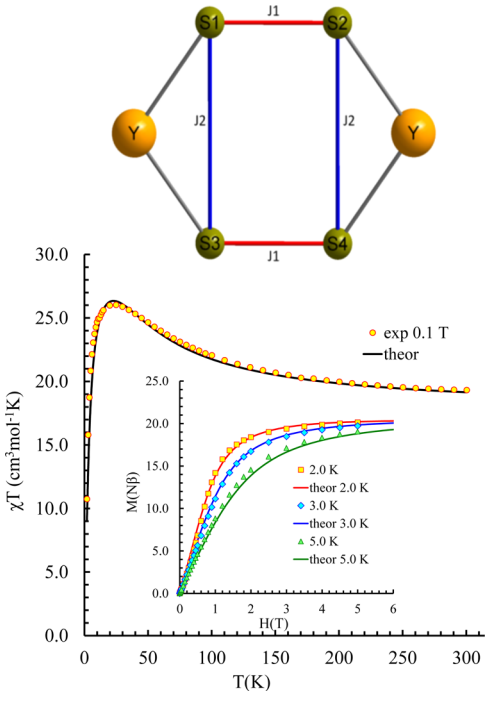

Figure 2. χT vs T of complex Fe_4Y_2 (**1**) and M vs H (inset). The solid lines are the best fit according to the Hamiltonian given in eq 1. Top: the spin model involved in the simulation.

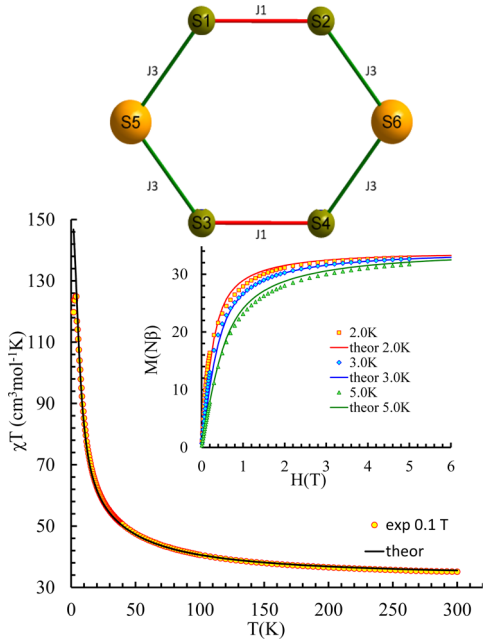

Figure 3. χT vs T of complex Fe_4Gd_2 (**2**) and M vs H (inset). The solid lines are the best fit according to the Hamiltonian given in eq 2. Top: The spin model involved in the simulation.

of χT is 124.60 cm^3 mol^{-1} K at around 4 K. At 2 K the susceptibility of Fe_4Gd_2 has a value of 119.77 cm^3 mol^{-1} K (Figure 3). The progressive increase in χT in nearly the whole temperature range (300−4 K) and the high values suggest the presence of dominant ferromagnetic interactions in **2**. Population of a high spin state at low temperature is also confirmed by magnetization measurements at 2, 3, and 5 K in the range 0−5 T (Figure 3).

The χT product of **3** (Fe_4Tb_2) has a room temperature value of 42.94 cm^3 mol^{-1} K which is close to the theoretical room temperature value of 45.85 cm^3 mol^{-1} K of four uncoupled Fe^{III} (d^5, S = 5/2, g = 2) and two Tb^{III} ($^7F_6$, g = 3/2, S = 3, L = 3, J = 6) ions. Upon cooling χT increases rapidly to reach a maximum of 132.29 cm^3 mol^{-1} K at 6.0 K. Below 6 K there is a drop to a value of 100.83 cm^3 mol^{-1} K at 2 K.

Complexes **4** (Fe_4Dy_2) and **5** (Fe_4Ho_2) behave in a similar fashion to **2** and **3**. At room temperature their susceptibility is at 44.71 cm^3 mol^{-1} K for **4** and 42.67 cm^3 mol^{-1} K for **5** which are in good agreement with the theoretical values of 45.85 cm^3 mol^{-1} K (Dy^{III} $^6H_{15/5}$, g = 4/3, S = 5/2, L = 5, J = 15/2) and 45.65 cm^3 mol^{-1}K (Ho^{III}, $^5I_8$, g = 5/4, S = 2, L = 6, J = 8). The maximum values are 155.86 cm^3 mol^{-1} K at 3.5 K for **4** and 136.20 cm^3 mol^{-1}K at around 4 K for **5**, respectively. At 2 K the susceptibility of Fe_4Ho_2 is 117.50 cm^3 mol^{-1} K and that of Fe_4Dy_2 is 136.86 cm^3 mol^{-1} K (Figure SI5). Similar to Fe_4Gd_2 (**2**) based on temperature dependence of χT, dominant ferromagnetic interactions are also present in compounds **3**−**5**. The magnetization measurements for complexes **3**−**5** are consistent with temperature dependence measurement and support a supposition about presence of ferromagnetic interaction in **3**−**5**.

According to the single crystal X-ray analysis, the core structure of Fe_4Y_2 (**1**) cluster has six bridged metallic centers. Allowing for the diamagnetism of the Y^{III} ions, the magnetic behavior of **1** can be simulated by a spin model involving four $S_{i,Fe}$, = 5/2 with two coupling constants (Figure 2). The isotropic Hamiltonian which describes this spin topology can be represented as follows:

$$\hat{H} = -2J_1(\hat{S}_{1,Fe}\cdot\hat{S}_{2,Fe} + \hat{S}_{3,Fe}\cdot\hat{S}_{4,Fe}) - 2J_2(\hat{S}_{1,Fe}\cdot\hat{S}_{3,Fe} + \hat{S}_{2,Fe}\cdot\hat{S}_{4,Fe}) \quad (1)$$

where $S_{i,Fe}$, refers to the spins 5/2 of the four Fe^{III} ions, J_1 corresponds to Fe^{III}−Fe^{III} coupling via the double azide bridge, and J_2 to the weak magnetic interaction via the bridge involving the diamagnetic Y^{III} ions (Figure 2).

The best fit for the experimental data is given by J_1 = +3.20 cm^{-1}, J_2 = −0.16 cm^{-1}, and g = 2.01 and J_1 = +3.20 cm^{-1}, J_2 = −0.15 cm^{-1}, and g = 2.04 respectively (Figure 2). As shown previously for Fe_2 dimers, the interaction via a double azide bridge is ferromagnetic.[32,41,42] The weak antiferromagnetic interaction (J_2) between two Fe_2 units across the diamagnetic Y^{III} ions is slightly lower than the value obtained in the case of Fe_4Lu_2 where the magnetic interaction is mediated by Lu^{III}.[32]

Compounds **2** and **1** are isostructural with identical Fe−N−Fe angles at the bridging azide ligands, and so we can expect similar values for the ferromagnetic interaction J_1 in **1** and **2**. In contrast to **1** in compound **2** the strongly paramagnetic Gd ions (S = 7/2) are present. In this case a new term J_3 should be introduced to define the interaction between Fe^{III} and Gd^{III} (Figure 3). Consequently, the Hamiltonian for which describes a cyclic spin model involving the four Fe^{III} and two Gd^{III} is

$$\hat{H} = -2J_1(\hat{S}_{1,Fe}\cdot\hat{S}_{2,Fe} + \hat{S}_{3,Fe}\cdot\hat{S}_{4,Fe}) - 2J_3(\hat{S}_{1,Fe}\cdot\hat{S}_{5,Gd} + \hat{S}_{4,Fe}\cdot\hat{S}_{6,Gd} + \hat{S}_{2,Fe}\cdot\hat{S}_{6,Gd} + \hat{S}_{3,Fe}\cdot\hat{S}_{5,Gd}) \quad (2)$$

where $S_{i,Gd}$ is the spin of a Gd ion S = 7/2, $S_{i,Fe}$, refer to the spins 5/2 of Fe^{III} ions, J_1 corresponds to the similar Fe^{III}−Fe^{III} coupling which should be similar to that in Fe_4Y_2, and J_3 to the magnetic interaction between Fe^{III}−Gd^{III} ions (Figure 3). The

DOI: 10.1021/acs.inorgchem.6b02682
Inorg. Chem. 2017, 56, 4796−4806

Table 1. Magnetic Data Extracted from the Plots of χT vs T (under 0.1 T) for Compounds 1−5

compounds	curie constant for each Ln ion at 300 K (cm^3K/mol)	χT (cm^3 K/mol) at 300 K, calc. from Curie constants	χT (cm^3 K/mol) at 300 K	T (K) of the max. value of χT	max value of χT (cm^3 K/mol)	χT (cm^3 K/mol) at 2 K
Fe_4Y_2 (**1**)		17.514	19.31	25.0	26.02	10.74
Fe_4Gd_2 (**2**)	7.87	33.25	35.07	4.0	124.60	119.77
Fe_4Tb_2 (**3**)	11.82	41.15	42.94	6.0	132.29	100.83
Fe_4Dy_2 (**4**)	14.17	45.85	44.71	3.5	155.86	136.86
Fe_4Ho_2 (**5**)	14.07	45.65	42.67	4.0	136.20	117.50

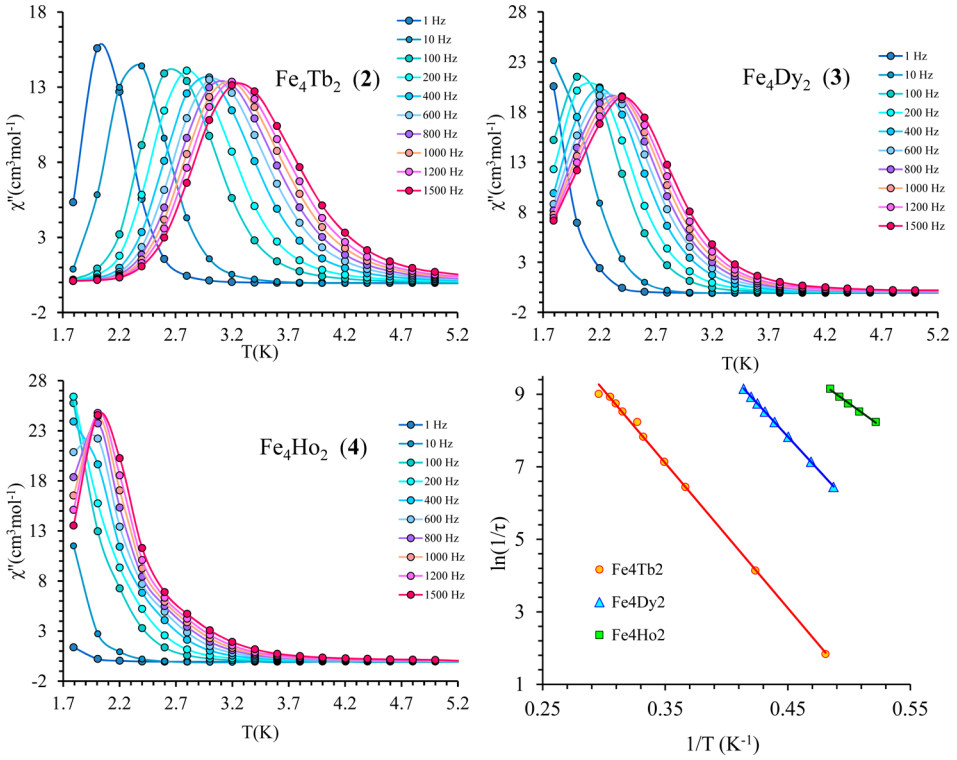

Figure 4. Out-of-phase susceptibility vs temperature at indicated frequencies for Fe_4Tb_2 (**3**), Fe_4Dy_2 (**4**), and Fe_4Ho_2 (**5**). Bottom right: Arrhenius plot for **3**−**5**. The continuous line corresponds to the fitting to an Arrhenius equation.

Table 2. ZFS Parameters, g Factor, and Magnetic Interaction Extracted from HF-EPR Spectra of 1−5[a]

Ln	g	ZFS (K)	D_{dim} (K)	J_{Fe-Ln} (K)	U_{eff}/k_b (K)	τ (10^{-10} s)
Y	2.00(5)	3.98[b]	−0.50(8)[c]			
Gd	1.98(2)	1.18(1)	−0.25(6)	0.58[d]		
Tb	2.00(4)	5.16(7)	−0.25(6)	0.25(5)	40.0	0.25 (6)
Dy	1.89(4)	4.88(8)	−0.25(6)	0.18(8)	36.9	6.8 (5)
Ho	1.92(7)	4.10(3)	−0.25(6)	0.12(8)	24.0	(4)

[a]Relaxation times and effective energy barriers of slow magnetic relaxation in complexes **3**−**5** based on the *ac* susceptibility analysis. [b]Energy difference between the ground state and the first excited state at 1.48 T. [c]Single ion anisotropy of Fe ion. [d]$J_{3(Fe-Gd)}$ is estimated from the temperature dependence of magnetic susceptibility measurements.

best fit for the χT product data corresponds to J_1 = 3.60 cm^{-1}, J_3 = 0.4 cm^{-1}, and g = 1.97 and for the magnetization data J_1 = 3.60 cm^{-1}, J_3 = 0.18 cm^{-1}, and g = 1.95. Accordingly at low temperatures a spin ground state value of S_T = 17 is dominant in **2**.

ac magnetic susceptibility measurements performed over a 2−10 K range and zero *dc* field using a 3.0 G *ac* oscillating field (1−1500 Hz) for compounds **3**−**5** are depicted in the Figure 4. These data show evident frequency dependent in- and out-of-phase signals below 5 K. The relaxation times at different temperatures were extracted from *ac* susceptibility data and were fitted to an Arrhenius law.

$$(1/\tau) = (1/\tau_0)e^{-U_{eff}/kT} \quad (3)$$

The characteristic relaxation time and energy barrier of slow magnetic relaxation of 40.0 K and 2.5 × 10^{-9} s for **3** (Fe_4Tb_2), 36.9 K and 6.8 × 10^{-10} s for **4** (Fe_4Dy_2) and 24.0 K and 8.0 × 10^{-10} s for **5** (Fe_4Ho_2) could be (Table 2).

It should be noted that presence of slow relaxation in Ho^{3+} compounds is relatively rare as a result of its comparatively isotropic ground state and indeed is the first Fe-Ln compound displaying SMM behavior for Ho^{3+}.[43−48] The heights of the energy barriers are in line with the increase in coupling strength between Fe^{III} and Ln^{III}. Furthermore, the Arrhenius plot of all

DOI: 10.1021/acs.inorgchem.6b02682
Inorg. Chem. 2017, 56, 4796−4806

three compounds showing slow relaxation can be displayed as a straight line that is showing no hints of tunneling or spin−lattice effects. No frequency-dependent *ac* signals in the out-of-phase component for compound **1** and **2** were observed.

HF-EPR. Figure 5 shows the EPR spectra of complex **1** (Fe_4Y_2) and complex **2** (Fe_4Gd_2) at various frequencies at 4 K.

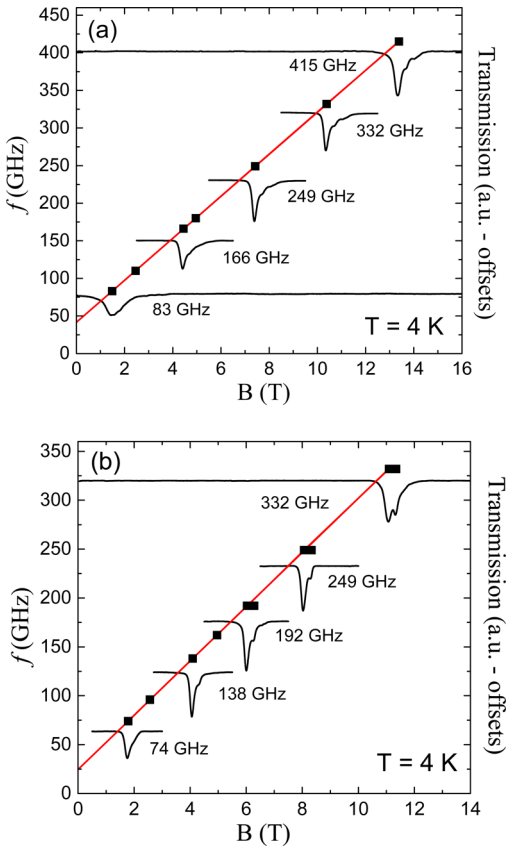

Figure 5. EPR spectra of complex **1** (a) and **2** (b) at 4 K and at various frequencies. Each spectrum is vertically shifted with an offset for a clear view. Squares represent the magnetic resonance fields. The red line is a linear fitting line extrapolated to the zero-field splitting.

The spectra of both complexes are similar in the whole magnetic field and temperature range under study. In both complexes, an asymmetric absorption signal is observed at low frequencies that develops a structure at the right shoulder with increasing the frequency/magnetic field. This suggests that the EPR signal consists of a main peak with the multiple overlapping peak of a smaller intensity at the high-field side. Remarkably, as can be seen in Figure 6, as the temperature increases from 4 K, the intensity of the main peak decreases, whereas the shoulder gains intensity and the total signal shifts to higher fields. Such a redistribution of the spectral weight accompanied by the shift of the spectrum gives evidence that the main EPR peak dominant at 4 K corresponds to the ground state excitation, and the right-side overlapping satellites are due to resonances within the thermally activated spin states of the complexes. As we focus on the characterization of the ground state properties, in the following only the main EPR peak will be considered.

The EPR spectra of complexes **3**−**5** (Fe_4Tb_2, Fe_4Dy_2, and Fe_4Ho_2) at various frequencies and 4 K are shown in Figure 7. Similarly to complexes **1** and **2**, a single peak is observed for complex **3** (Fe_4Tb_2) and complex **5** (Fe_4Ho_2), but the peak

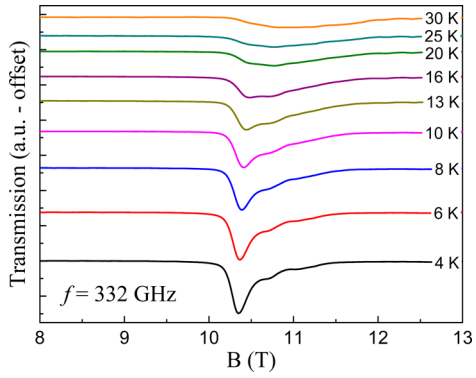

Figure 6. EPR spectra of complex **1** at 332 GHz upon variation of the temperature.

width is much broader for these latter complexes. For complex **3**, two distinct peaks are observed indicating a larger separation of the overlapping peaks. Small additional features around the strong peaks in the spectra presumably arise from slight misalignment of the powder particles self-oriented in the magnetic field. In any case, for the three complexes **3**−**5**, the temperature dependence of the main peak dominating the spectrum at low temperatures (Figure S3) again gives evidence that it corresponds to the ground state resonance, as for complexes **1** and **2**. It can be noted that in the temperature dependence of the two peaks of complex **4**, the spectral weight is shifted from the peak at lower field to the peak at higher field as temperature increases, implying that the resonance at higher field is an excited state resonance. The peak features merge to a single peak as the temperature increases.

The ground state resonance position, at 4 K, is shown as squares in the frequency versus magnetic field diagrams (Figures 5 and 7). Linear fitting of the resonance positions allows estimating the *g*-values and the zero-field splittings (ZFS) of the complexes under study (see Table 2). Concerning the interpretation of the resulting ZFS values, complex **1** somehow differs from the other complexes since, in the complexes **2**−**5**, the extracted ZFS is associated with the excitation between the ground state and the first excited state. In complex **1** (Fe_4Y_2), there are only small antiferromagnetic interactions present in the material so that the ground spin state at around zero field is not well separated from the excited states. The experimentally observed ZFS hence cannot be associated with the energy difference between the ground state and the first excited one, and we hence do not consider the zero field gap of the linearly fitted resonance branch in complex **1** for the further analysis. Instead, the data at high frequency up to f = 415 GHz where the magnetic field is supposed to lift the zero field degeneracy were used to estimate the anisotropy of the Fe^{III} ions. To be specific, the EPR resonance branch of complex **1** was simulated using the matrix diagonalization method with an appropriate Heisenberg Hamiltonian. Since the Y^{III} ions are diamagnetic, the Hamiltonian for complex **1** can be written as a Hamiltonian involving four Fe ions:

$$\hat{H} = -g_{Fe}\mu_B \sum_i^4 \hat{B}\cdot\hat{S}_{i,Fe} + d_{Fe}\sum_i^4 (\hat{S}_{i,Fe}^z)^2 - 2J_1(\hat{S}_{1,Fe}\cdot\hat{S}_{2,Fe} + \hat{S}_{3,Fe}\cdot\hat{S}_{4,Fe}) - 2J_2(\hat{S}_{1,Fe}\cdot\hat{S}_{4,Fe} + \hat{S}_{2,Fe}\cdot\hat{S}_{3,Fe}) \quad (4)$$

DOI: 10.1021/acs.inorgchem.6b02682
Inorg. Chem. 2017, 56, 4796−4806

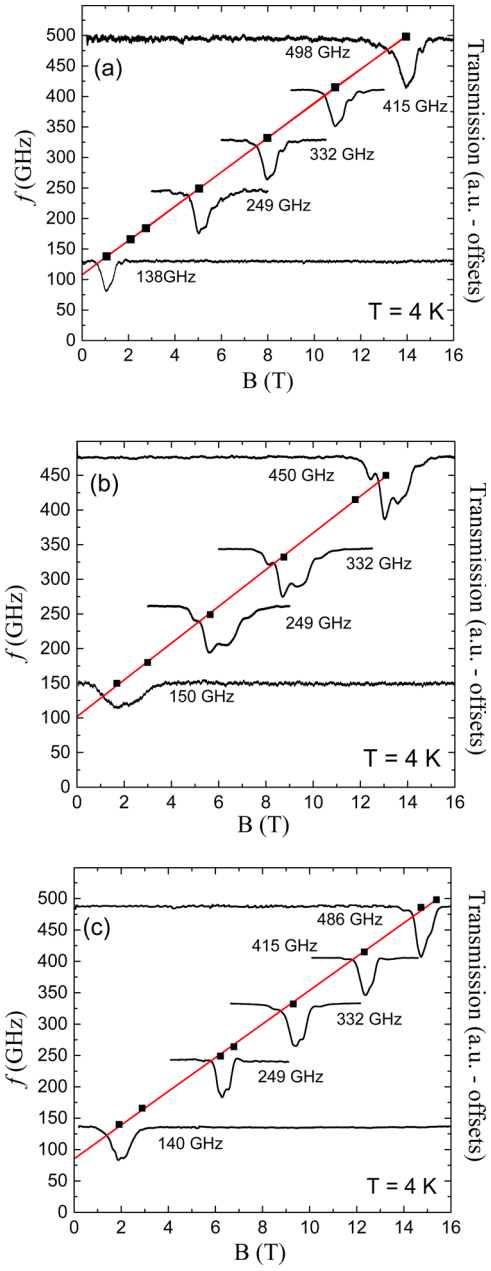

Figure 7. EPR spectra of complex **3** (a), **4** (b), and **5** (c) at 4 K and at various frequency. Each spectrum is vertically shifted with an offset for a clear view. Squares represent the magnetic resonance fields. The red line is a linear fitting line extrapolated to the zero-field splitting.

The first term is a Zeeman term and the second term comprises the anisotropy terms of the Fe^{III} ions. g_{Fe} represents the g-value of the Fe^{III} ion, μ_B the Bohr magneton, $\hat{B}$ the external magnetic field, and $\hat{S}_{i,Fe}$ the spin state matrix of ith Fe ion, respectively. d_{Fe} represents the anisotropy of the Fe ion. The third and fourth terms are the exchange interaction terms; J_1 is the exchange interaction between the Fe ions coupled by two azide anions, and J_2 is the exchange interaction between the Fe ions coupled through the Y ion. From the static magnetization data, the exchange interaction values are estimated; J_1 = 4.60 K, and J_2 = −0.23 K. The best simulation of the ground state resonance of complex **1** using the eq 1 provides the single ion anisotropy value of the Fe^{III} ion amounting to d_{Fe} = −0.50(8) K.

The Hamiltonian for complex **2** is different from the one for complex **1**. Since the Gd^{III} ions have a nonzero spin quantum number, S = 7/2, the dimension of the spin state matrix for the complex is much larger (82944*82944) than the one for complex **1**. In order to reduce the dimension of the spin state matrix, two Fe^{III} ions coupled by J_1 are treated as a ferromagnetic dimer with S_{dim} = 5. Since J_1 is the dominating and ferromagnetic exchange interaction, the dimer approximation is well justified. The Hamiltonian with the Fe^{III} dimers reads as follows:

$$\hat{H} = -g_{Fe}\mu_B \sum_{i}^{2} \hat{B}\cdot\hat{S}_{i,dim} - g_{Gd}\mu_B \sum_{i}^{2} \hat{B}\cdot\hat{S}_{i,Gd} + D_{dim} \sum_{i}^{2} (\hat{S}^{z}_{i,dim})^2 - 2J_{Fe-Gd} \sum_{i,j}^{2} \hat{S}_{i,dim}\cdot\hat{S}_{j,Gd} \quad (5)$$

$\hat{S}_{i,dim}$ and D_{dim} represent the spin state matrix and the anisotropy value of the Fe^{III} dimer, respectively. The anisotropy of the Gd^{III} ion is assumed to be negligible in this Hamiltonian, but this is not the case for the Fe^{III} ions. The exchange interaction between the Fe^{III} and Gd^{III} ions is estimated from the static magnetization to be J_{Fe-Gd} = 0.57 K. The best simulation of ZFS of complex **2** allows us to estimate the anisotropy value of the Fe^{III} dimer, D_{dim} = −0.25(6) K. This value compares well with the estimate obtained, D_{dim} = −0.28(8) K, considering the single ion anisotropy of Fe ions and the contribution to anisotropy due to the magnetic dipole−dipole interaction.[49]

The magnetic coupling constants $J_{Fe\text{-}Ln}$ (= J_3) of complexes **3**, **4**, and **5** (Fe_4Tb_2, Fe_4Dy_2, and Fe_4Ho_2) can be extracted from the ZFS observed in the EPR spectra. Because of the unquenched orbital contribution in lanthanide ions, the Hamiltonian should be modified by the Ising spin concept. In this approach, the Ising-type spin Hamiltonian for complexes **3**, **4**, and **5** can be written as follows:

$$\hat{H} = -g_{Fe}\mu_B \sum_{i}^{2} \hat{B}\cdot\hat{S}_{i,dim} - g_{Ln}\mu_B \sum_{i}^{2} \hat{B}^{z}\cdot\hat{J}^{z}_{i,Ln} + D_{dim} \sum_{i}^{2} (\hat{S}^{z}_{i,dim})^2 - 2J_{Fe-Ln} \sum_{i,j}^{2} \hat{S}^{z}_{i,dim}\cdot\hat{J}^{z}_{j,Ln} \quad (6)$$

In order to reduce the matrix dimension, the Fe dimer approximation was applied again. Since the Fe_4Ln_2 complexes are isostructural, D_{dim} = −0.25(6) K of complex **2** can be used for the ZFS simulation of other complexes. For an Ising spin, the z-axis projection of the J operator was used for the lanthanide ions in the Hamiltonian. We use the maximum of the total angular momentum value for the ground state of the lanthanide ions, i.e., J_{Tb}^{z} = ± 6, J_{Dy}^{z} = ± 15/2, and J_{Ho}^{z} = ± 8. The J_{Fe-Ln} values obtained from the best simulation of the ZFS values for complexes **3**, **4**, and **5** are shown in the Table 2.

There are few HF-EPR studies on the interaction between 4f and 3d ions. However, the ferromagnetic exchange interaction between Cu^{II} and Ln^{III} ions has been well studied.[27,50,51] For a Gd_2Cu_4 complex, Kahn et al.[50] proposed a superexchange-like mechanism with an excited state where the unpaired 3d electron of the Cu^{II} ion is transferred to the unoccupied 5d orbital of the 4f ions, i.e., $4f^7 5d^0\text{-}3d^9 \rightarrow 4f^7 5d^1\text{-}3d^8$ for the Gd^{3+}-Cu^{2+} electronic configuration. In this scenario, Hund's coupling favors the high spin $4f^7 5d^1\text{-}3d^8$ configuration of the excited state and hence ferromagnetic interaction between Cu and Gd

DOI: 10.1021/acs.inorgchem.6b02682
Inorg. Chem. 2017, 56, 4796−4806

moments in Gd_2Cu_4. For Ln ions in general, this model implies that the magnetic interaction between Cu and Ln ions depends on the number of 4f electrons. When the 4f shell is more than half full, the orbital momentum is parallel to spin momentum, $J = L + S$. Thus, the heavier Ln ions than Gd have a ferromagnetic interaction with Cu^{II} ion as in the case of Gd_2Cu_4. A weak ferromagnetic interaction between Cu^{II} and Dy^{III} ions $J_{Dy-Cu} = 1.4$ K has indeed been recently found by means of ab initio calculations on a Cu_5Dy_4 cluster.[56] In contrast, antiferromagnetic interaction is suggested by this model for lighter Ln ions since the total momentum is antiparallel to the total 4f-spin moment in that case. Similar arguments apply for the ferromagnetic interaction between Fe and Ln ions in the Fe_4Ln_2 complexes. It is noteworthy, however, that J_{Fe-Ln} is weaker than J_{Cu-Ln}. Upon variation of the Ln ions, J_{Fe-Ln} shows a consistent tendency with the effective barrier and depends on the atom number of Ln ions; $J_{Fe-Gd} > J_{Fe-Tb} > J_{Fe-Dy} > J_{Fe-Ho}$. Figure 8 displays J_{Fe-Ln} for the

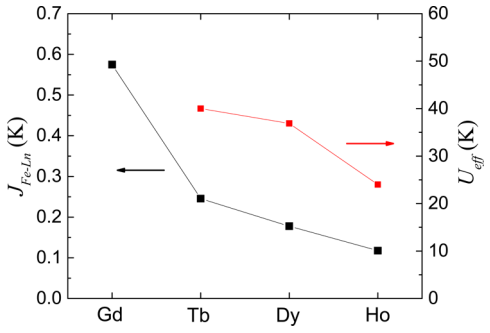

Figure 8. Exchange interaction between Fe and Ln moments and effective anisotropy barrier for the studied Ln ions.

studied lanthanide ions. Complex **2** has the largest J_{Fe-Ln} coupling and as the atom number of lanthanide ions increases, J_{Fe-Ln} decreases. Quantitatively, J_{Cu-Gd} is 6.9 K in GdCu[51] and 8.6 K in Cu_4Gd_2,[50] while our study yields $J_{Fe-Gd} = 0.57$ K. This difference may be associated with the different electronic configuration, i.e., $3d^5$ in Fe^{III} vs $3d^9$ in Cu^{II}, as due to shielding effects the above-mentioned excitation process may be favored in Cu^{II} as compared to Fe^{III}. In the competition between the charge transfer energy and the localization energy, the Fe^{III} ion has stronger localization energy than the Cu^{II} ion resulting in the weaker exchange interaction. Furthermore, the structure distortion also might contribute to the weaker exchange interaction. Since the orbital overlap is crucial in Kahn's model,[50] orbital misalignment present in the complexes under study might critically weaken the ferromagnetic interaction between Fe and Ln ions as well.

The atom number dependence of J_{Fe-Ln} can be explained in the scenario of Kahn et al. as well, if the reduced number of unpaired spins is considered. For $Z > 64$, the number of unpaired 4f electrons and hence Hund's coupling in the excited configuration $4f^n5d^1$ ($7 < n < 14$) is smaller than for $n = 7$, which causes reduced ferromagnetic interaction.[50,51] Interestingly, the effective barrier has the same atom number dependence as J_{Fe-Ln}. This observation is inconsistent with the expected anisotropy of lanthanide ions, i.e., Dy > Tb > Ho ≫ Gd.[52]

Mössbauer Spectral Studies. In order to investigate the relaxation rates further, ^{57}Fe Mössbauer spectroscopy was employed. The decay rate of the ^{57}Fe excited state is in the range of $\sim 10^{-7}$ s and by that order of magnitude faster than the *ac* frequency of the magnetic susceptibility measurements. With this technique it is possible to detect slow magnetic relaxation even in samples that do not show an out-of-phase signal in the *ac* susceptibility measurements over the same temperature range. Mössbauer spectra (MS) of powdered samples of compounds **1**–**6** were recorded at temperatures between 85 and 3 K (Figures 9 and Supporting Information).

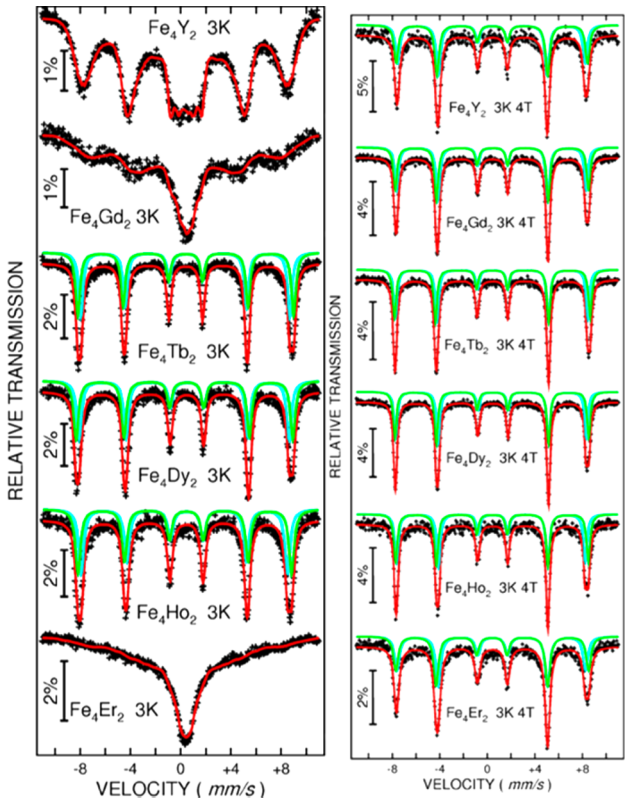

Figure 9. Mössbauer spectra of **1**–**6** obtained at 3 K (left) and at 3 K in an applied field of 4 T (right). The green lines indicate the fit.

Compound **1** (Fe_4Y_2) containing the diamagnetic Y^{3+} shows an intermediate relaxation rate. Since the structural differences between the Fe^{III} sites are very small, the fit of the Mössbauer spectra was done using one doublet. The spectra of compound **1** at all temperatures are dominated by the relaxation at intermediate rate. Compounds **2**–**6** all show a quadrupole doublet between 85 and 30 K with no hyperfine splitting observable. The values obtained for the isomer shift (δ) and quadrupole splitting (ΔE_Q) at 30 K for compound **4** were used to fit the magnetic spectra for **1** at 3 K in applied external magnetic fields.

The spectra of **1** and **2** (Fe_4Y_2 and Fe_4Gd_2) at 3 K show line characteristics of relaxations at the intermediate rate, being considerably broadened, with wings that spread from about −8 to +8 mm/s with broad absorption peaks at the center of the spectra. That of **1** (Fe_4Y_2) shows intermediate relaxation speeds relative to the Mössbauer time scale. Since the only paramagnetic ions in the complex responsible for this behavior are the Fe^{III} ions, here the combination of a high spin ground state ($S = 5$) and a small negative zero field splitting is responsible for a small energy barrier against the reversal of magnetization. The spectrum of **2** shows that the Fe^{III} ions are relaxing faster than those in **1**. The interaction of the Fe_2 unit

DOI: 10.1021/acs.inorgchem.6b02682
Inorg. Chem. 2017, 56, 4796−4806

with the isotropic Gd^{III} ion has no orientational restraints on its spin and so can relax very fast, thus also speeding up the relaxation of the Fe^{III}. By contrast, compounds **3**−**5** (Fe_4Tb_2, Fe_4Dy_2, and Fe_4Ho_2) show well-defined magnetic spectra with the characteristic six absorption lines at 3 K (Figure 9, left), indicating that the spin-relaxation time has now slowed down with respect to the Mössbauer time scale.

All magnetic spectra for **3**−**5** were fitted with two sextets to take into account the slight differences in the local symmetries and hyperfine internal magnetic fields on the two Fe^{III} ions. In these compounds containing paramagnetic lanthanides favoring relaxation through an easy axis (Fe_4Tb_2, Fe_4Dy_2, and Fe_4Ho_2), the crystal field stabilizes the highest m_j state of each lanthanide. The interaction of such a state with the Fe_2 units creates a high energy barrier against the reversal of magnetization and thus creating a Zeeman splitting of the Fe nuclear spins in the absence of any applied field. In effect, these lanthanides pin the Fe^{III} spins, thus decreasing their relaxation rate. This is in line with the results observed in the *ac* susceptibility measurements. For **6** (Fe_4Er_2) the magnetic spectra, in contrast to all other compounds, show only a single broad feature. In the case of Er the ligand field now destabilizes the highest m_j state. The interaction of this ion with the Fe_2 unit increases the magnetic relaxation rate of the Fe^{III} ions even more effectively than the Gd ion does in compound **2**.

It is instructive to see how the Mössbauer spectra are affected on application of strong *dc* fields. Spectra were measured at 3 K for all compounds in external fields of 1−5 T (Figure 9 (right), Figure S1 and Figure S2). For ferromagnetic materials, alignments along external fields B_{ext}, with a simultaneous rotation of the internal field are expected, resulting in a reduction of the nuclear magnetic field. As can be seen from the spectra at 4 T (Figure 9) compared with the 2 T spectra the energies of the first and sixth peaks of both sextets of each spectrum move inward and the effective field is slightly reduced. This indicates that in all compounds the intramolecular Fe−Fe interaction is ferromagnetic.[53]

The ferromagnetic interaction between the Fe^{III} ions allows these to be easily aligned with an applied field, in contrast to the situation where the Fe^{III} are antiferromagnetically coupled.[54] Comparing the Mössbauer spectrum of compound **1** with compounds **2**−**6** it is clear that under these applied fields, the rare earth ion no longer has any perceptible influence on the nature of the spectra and thus on the hyperfine field at the Fe^{III}.

CONCLUSIONS

In summary we present the synthesis, structure, magnetic properties, as well as the Mössbauer- and EPR studies of a ring-shaped $[Fe^{III}_4Ln^{III}_2(Htea)_4(\mu\text{-}N_3)_4(N_3)_3(piv)_3]$ (Ln = Y **1**, Gd **2**, Tb **3**, Dy **4**, Ho **5**, Er **6**) coordination cluster. The Dy, Tb, and Ho analogues show blocking of the magnetization at low temperatures without applied fields. The anisotropy of the 3d ion and the exchange interaction between 3d and 4f ions in Fe_4Ln_2 complexes are unambiguously determined by HF-EPR measurements at low temperature. Ferromagnetic exchange interaction J_{Fe-Ln} is found which decreases upon variation of the Ln ions to larger atomic numbers. This dependence is similar to the behavior shown in the effective barrier values of complex **3**−**5**. Further information about the anisotropy of the Ln^{3+} ions was gathered with ^{57}Fe Mössbauer spectroscopy. At 3 K spin blocking was found to occur in complex **3**−**5** in the Mössbauer time window in agreement with the SMM behavior demonstrated by the ac susceptibility measurements. At this temperature, the spectra for Fe_4Y_2 and Fe_4Gd_2 only show an onset of relaxation at an intermediate rate. The reason for this behavior lies in the large and uniaxial anisotropy of Tb, Dy, and Ho ions, the isotropic character of the Gd and the diamagnetic ground state for the Y ions. In the case of the Er^{III} compound, the easy plane anisotropy leads to the fastest relaxation of the Fe^{III} nuclear spin. At 3 K spin blocking was found to occur in complexes **3**−**5** in the Mössbauer time window in accord with the SMM behavior demonstrated by the *ac* susceptibility measurements. From the consistent behavior of J_{Fe-Ln} and effective barrier, the exchange interaction between 3d and 4f ions should be considered as an important factor in the enhancement of SMM characteristics in 3d 4f complexes.

ASSOCIATED CONTENT

Supporting Information

The Supporting Information is available free of charge on the ACS Publications website at DOI: 10.1021/acs.inorgchem.6b02682.

Additional Mössbauer spectra and magnetic data (PDF)
Crystallographic data (CIF1, CIF2, CIF3, CIF4, CIF5)

AUTHOR INFORMATION

Corresponding Authors

*(R.K.) E-mail: ruediger.klingeler@kip.uni-heidelberg.de.
*(A.K.P.) E-mail: annie.powell@kit.edu.

ORCID

Annie K. Powell: 0000-0003-3944-7427

Notes

The authors declare no competing financial interest.

ACKNOWLEDGMENTS

The work was supported in part by the Deutsche Forschungsgemeinschaft through the Projects FOR1154 “Towards Molecular Spintronics” and INST 35/1085-1 FUGG and TR-SFB 88 “3MET”. V.M., D.P., and G.N. also thank the Alexander von Humboldt Foundation (V.M., D.P., and G.N.) for financial support.

REFERENCES

(1) Vincent, R.; Klyatskaya, S.; Ruben, M.; Wernsdorfer, W.; Balestro, F. Electronic read-out of a single nuclear spin using a molecular spin transistor. *Nature* **2012**, *488*, 357−360.

(2) Bogani, L.; Wernsdorfer, W. Molecular spintronics using single-molecule magnets. *Nat. Mater.* **2008**, *7*, 179−186.

(3) Aromí, G.; Aguilà, D.; Gamez, P.; Luis, F.; Roubeau, O. Design of magnetic coordination complexes for quantum computing. *Chem. Soc. Rev.* **2012**, *41*, 537−546.

(4) Sessoli, R.; Gatteschi, D.; Caneschi, A.; Novak, M. A. Magnetic bistability in a metal-ion cluster. *Nature* **1993**, *365*, 141−143.

(5) Lis, T. Preparation, Structure, and Magnetic Properties of a Dodeeanuelear Mixed-Valence Manganese Carboxylate. *Acta Crystallogr., Sect. B: Struct. Crystallogr. Cryst. Chem.* **1980**, *36*, 2042−2046.

(6) Sessoli, R.; Tsai, H.-L.; Schake, A. R.; Wang, S.; Vincent, J. B.; Folting, K.; Gatteschi, D.; Christou, G.; Hendrickson, D. N. High Spin Molecules:$[Mn_{12}O_{12}(O_2CR)_{16}(H_2O)_4]$. *J. Am. Chem. Soc.* **1993**, *115*, 1804−1816.

(7) Caneschi, A.; Gatteschi, D.; Sessoli, R.; Barra, A. L.; Brunel, L. C.; Guillot, M. Alternating Current Susceptibility, High Field Magnetization and Millimeter Band EPR Evidence for a Ground S = 10 State in $[Mn_{12}O_{12}(CH_3COO)_{16}(H_2O)_4]_2CHCOOH_4H_2O$. *J. Am. Chem. Soc.* **1991**, *113*, 5873−5874.

DOI: 10.1021/acs.inorgchem.6b02682
Inorg. Chem. 2017, 56, 4796−4806

(8) Osa, S.; Kido, T.; Matsumoto, N.; Re, N.; Pochaba, A.; Mrozinski, J. A tetranuclear 3d-4f single molecule magnet: $[Cu^{II}LTb^{III}(hfac)_2]_2$. *J. Am. Chem. Soc.* **2004**, *126*, 420−421.
(9) Liu, J.; Chen, Y.-C.; Jia, J.-H.; Liu, J.-L.; Vieru, V.; Ungur, L.; Chibotaru, L. F.; Lan, Y.; Wernsdorfer, W.; Gao, S.; Chen, X.-M.; Tong, M.-L. A Stable Pentagonal-Bipyramidal Dy(III) Single-Ion Magnet with a Record Magnetization Reversal Barrier over 1000 K. *J. Am. Chem. Soc.* **2016**, *138*, 5441−5450.
(10) Chen, Y.-C.; Liu, J.-L.; Ungur, L.; Liu, J.; Li, Q.-W.; Wang, L.-F.; Ni, Z.-P.; Chibotaru, L. F.; Chen, X.-M.; Tong, M.-L. *J. Am. Chem. Soc.* **2016**, *138*, 2829−2837.
(11) Rinehart, J. D.; Fang, M.; Evans, W. J.; Long, J. R. Strong exchange and magnetic blocking in N_2^{3-}-radical-bridged lanthanide complexes. *Nat. Chem.* **2011**, *3*, 538−542.
(12) Meihaus, K. R.; Long, J. R. Magnetic blocking at 10 K and a Dipolar-mediated avalanche in salts of the bis(η8-cyclooctatetraenide) complex $[Er(COT)_2]^-$. *J. Am. Chem. Soc.* **2013**, *135*, 17952−17957.
(13) Le Roy, J. J.; Ungur, L.; Korobkov, I.; Chibotaru, L. F.; Murugesu, M. Coupling Strategies to Enhance Single-Molecule Magnet Properties of Erbium−Cyclooctatetraenyl Complexes. *J. Am. Chem. Soc.* **2014**, *136*, 8003−8010.
(14) Liddle, S. T.; van Slageren, J. Improving f-element single molecule magnets. *Chem. Soc. Rev.* **2015**, *44*, 6655−6669.
(15) Blagg, R. J.; Ungur, L.; Tuna, F.; Speak, J.; Comar, P.; Collison, D.; Wernsdorfer, W.; McInnes, E. J. L.; Chibotaru, L. F.; Winpenny, R. E. P. Magnetic relaxation pathways in lanthanide single-molecule magnets. *Nat. Chem.* **2013**, *5*, 673−678.
(16) Gregson, M.; Chilton, N. F.; Ariciu, A.-M.; Tuna, F.; Crowe, I. F.; Lewis, W.; Blake, A. J.; Collison, D.; McInnes, E. J. L.; Winpenny, R. E. P.; Liddle, S. T. A monometallic lanthanide bis(methanediide) single molecule magnet with a large energy barrier and complex spin relaxation behaviour. *Chem. Sci.* **2016**, *7*, 155−165.
(17) Langley, S. K.; Wielechowski, D. P.; Vieru, V.; Chilton, N. F.; Moubaraki, B.; Abrahams, B. F.; Chibotaru, L. F.; Murray, K. S. A $\{Cr^{III}_2Dy^{III}_2\}$ Single-Molecule Magnet: Enhancing the Blocking Temperature through 3d Magnetic Exchange. *Angew. Chem.* **2013**, *125*, 12236−12241.
(18) Liu, J.-L.; Guo, F.-S.; Meng, Z.-S.; Zheng, Y.-Z.; Leng, J.-D.; Tong, M.-L.; Ungur, L.; Chibotaru, L. F.; Heroux, K. J.; Hendrickson, D. N. Symmetry related $[Dy^{III}_6Mn^{III}_{12}]$ cores with different magnetic anisotropies. *Chem. Sci.* **2011**, *2*, 1268−1272.
(19) Rinck, J.; Novitchi, G.; Van den Heuvel, W.; Ungur, L.; Lan, Y.; Wernsdorfer, W.; Anson, C. E.; Chibotaru, L. F.; Powell, A. K. Ein achtkerniger $[Cr^{III}_4Dy^{III}_4]$-3d-4f-Einzelmolekülmagnet. *Angew. Chem.* **2010**, *122*, 7746−7750.
(20) Liu, J.-L.; Wu, J.-Y.; Chen, Y.-C.; Mereacre, V.; Powell, A. K.; Ungur, L.; Chibotaru, L. F.; Chen, X.-M.; Tong, M.-L. Ein heterometallischer Fe^{II} -Dy^{III} -Einzelmolekülmagnet mit Rekord-Anisotropiebarriere. *Angew. Chem.* **2014**, *126*, 13180−13184.
(21) Mondal, K. C.; Sundt, A.; Lan, Y.; Kostakis, G. E.; Waldmann, O.; Ungur, L.; Chibotaru, L. F.; Anson, C. E.; Powell, A. K. Coexistence of Distinct Single-Ion and Exchange-Based Mechanisms for Blocking of Magnetization in a $Co^{II}_2Dy^{III}_2$ Single-Molecule Magnet. *Angew. Chem.* **2012**, *124*, 7668−7672.
(22) Liu, J.-L.; Wu, J.-Y.; Huang, G.-Z.; Chen, Y.-C.; Jia, J.-H.; Ungur, L.; Chibotaru, L. F.; Chen, X.-M.; Tong, M.-L. Desolvation-Driven 100-Fold Slow-down of Tunneling Relaxation Rate in Co(II)-Dy(III) Single-Molecule Magnets through a Single-Crystal-to-Single-Crystal Process. *Sci. Rep.* **2015**, *5*, 16621.
(23) Kühne, I. A.; Magnani, N.; Mereacre, V.; Wernsdorfer, W.; Anson, C. E.; Powell, A. K. An octanuclear $\{Cu(II)_4Dy(III)_4\}$ coordination cluster showing single molecule magnet behaviour from field accessible states. *Chem. Commun.* **2014**, *50*, 1882−1885.
(24) Okazawa, A.; Shimada, T.; Kojima, N.; Yoshii, S.; Nojiri, H.; Ishida, T. Exchange coupling and its chemical trend studied by high-frequency EPR on heterometallic $[Ln_2Ni]$ complexes. *Inorg. Chem.* **2013**, *52*, 13351−13355.
(25) Mossin, S.; Tran, B. L.; Adhikari, D.; Pink, M.; Heinemann, F. W.; Sutter, J.; Szilagyi, R. K.; Meyer, K.; Mindiola, D. J. A Mononuclear Fe (III) Single Molecule Magnet With a 3/2↔5/2 Spin Crossover. *J. Am. Chem. Soc.* **2012**, *134*, 13651−13661.
(26) Rechkemmer, Y.; Fischer, J. E.; Marx, R.; Dörfel, M.; Neugebauer, P.; Horvath, S.; Gysler, M.; Brock-Nannestad, T.; Frey, W.; Reid, M. F.; Van Slageren, J. Comprehensive spectroscopic determination of the crystal field splitting in an erbium single-ion magnet. *J. Am. Chem. Soc.* **2015**, *137*, 13114−13120.
(27) Shimada, T.; Okazawa, A.; Kojima, N.; Yoshii, S.; Nojiri, H.; Ishida, T. Ferromagnetic Exchange Couplings Showing a Chemical Trend in Cu-Ln-Cu Complexes (Ln = Gd, Tb, Dy, Ho, Er). *Inorg. Chem.* **2011**, *50*, 10555−10557.
(28) Pedersen, K. S.; Ariciu, A.-M.; McAdams, S.; Weihe, H.; Bendix, J.; Tuna, F.; Piligkos, S. Toward Molecular 4f Single-Ion Magnet Qubits. *J. Am. Chem. Soc.* **2016**, *138*, 5801−5804.
(29) Pedersen, K. S.; Ungur, L.; Sigrist, M.; Sundt, A.; Schau-Magnussen, M.; Vieru, V.; Mutka, H.; Rols, S.; Weihe, H.; Waldmann, O.; Chibotaru, L. F.; Bendix, J.; Dreiser, J. Modifying the properties of 4f single-ion magnets by peripheral ligand functionalisation. *Chem. Sci.* **2014**, *5*, 1650−1660.
(30) Okazawa, A.; Nogami, T.; Nojiri, H.; Ishida, T. Exchange Coupling and Energy-Level Crossing in a Magnetic Chain $[Dy_2Cu_2]$ n Evaluated by High-Frequency Electron Paramagnetic Resonance. *Chem. Mater.* **2008**, *20*, 3110−3119.
(31) Gysler, M.; El Hallak, F.; Ungur, L.; Marx, R.; Hakl, M.; Neugebauer, P.; Rechkemmer, Y.; Lan, Y.; Sheikin, I.; Orlita, M.; Anson, C. E.; Powell, A. K.; Sessoli, R.; Chibotaru, L. F.; van Slageren, J. Multitechnique investigation of Dy 3 − implications for coupled lanthanide clusters. *Chem. Sci.* **2016**, *7*, 4347−4354.
(32) Schmidt, S.; Prodius, D.; Novitchi, G.; Mereacre, V.; Kostakis, G. E.; Powell, A. K. Ferromagnetic heteronuclear $\{Fe_4(Er,Lu)_2\}$ cyclic coordination clusters based on ferric wheels. *Chem. Commun.* **2012**, *48*, 9825−9827.
(33) Sheldrick, G. M. Crystal structure refinement with SHELXL. *Acta Crystallogr., Sect. C: Struct. Chem.* **2015**, *71*, 3−8.
(34) Sheldrick, G. M. SHELXT − Integrated space-group and crystal-structure determination. *Acta Crystallogr., Sect. A: Found. Adv.* **2015**, *71*, 3−8.
(35) Sheldrick, G. M. *SHELXTL 6.12*; Bruker AXS: Madison, WI, 2003.
(36) Kahn, O. *Molecular Magnetism*, 1st ed.; John Wiley & Sons: Cambridge, 1993.
(37) Pascal, P. Recherches Magnétochimiques. *Ann. Chim. Phys.* **1910**, *19*, 5.
(38) Borras-Almenar, J. J.; Clemente-Juan, J. M.; Coronado, E.; Tsukerblat, B. S. J. MAGPACK A Package to Calculate the Energy Levels, Bulk Magnetic Properties, and Inelastic Neutron Scattering Spectra of High Nuclearity Spin Clusters. *J. Comput. Chem.* **2001**, *22*, 985−991.
(39) Golze, C.; Alfonsov, A.; Klingeler, R.; Büchner, B.; Kataev, V.; Mennerich, C.; Klauss, H.-H.; Goiran, M.; Broto, J.-M.; Rakoto, H.; Demeshko, S.; Leibeling, G.; Meyer, F. Tuning the magnetic ground state of a tetranuclear nickel(II) molecular complex by high magnetic fields. *Phys. Rev. B: Condens. Matter Mater. Phys.* **2006**, *73*, 224403.
(40) Ako, A. M.; Burger, B.; Lan, Y.; Mereacre, V.; Clerac, R.; Buth, G.; Gomez-Coca, S.; Ruiz, E.; Anson, C. E.; Powell, A. K. Magnetic Interactions Mediated by Diamagnetic Cations in $[Mn_{18}M]$ (M= Sr^{2+}, Y^{3+}, Cd^{2+} and Lu^{3+}) Coordination Clusters. *Inorg. Chem.* **2013**, *52*, 5764−5774.
(41) De Munno, G.; Poerio, T.; Viau, G.; Julve, M.; Lloret, F.; Journaux, Y.; Riviee, E. New magnetic behaviour of honeycomb layered compounds. Crystal structures of $[M_2(bipym)(N_3)_4]$(M = Co, Fe; bipym = 2,2′-bipyrimidine). *Chem. Commun.* **1996**, *2*, 2587−2588.
(42) De Munno, G.; Poerio, T.; Viau, G.; Julve, M.; Lloret, F. Ferromagnetic Coupling in the Bis(μ-end-on-azido)iron(III) dinuclear complex. Anion of Fe(II) $(bpym)_3]_2[Fe_2(III)(N_3)_{10}]2H_2O$. *Angew. Chem., Int. Ed. Engl.* **1997**, *36*, 1459−1461.
(43) Mereacre, V.; Lan, Y.; Clérac, R.; Ako, A. M.; Hewitt, I. J.; Wernsdorfer, W.; Buth, G.; Anson, C. E.; Powell, A. K. A Family of

DOI: 10.1021/acs.inorgchem.6b02682
Inorg. Chem. 2017, 56, 4796−4806

$Mn^{III}_2Ln_2(\mu_4$ -O) Compounds: Synthesis, Structures, and Magnetic Properties. *Inorg. Chem.* **2010**, *49*, 5293−5302.
(44) Zhao, L.; Wu, J.; Ke, H.; Tang, J. A Family of Defect-dicubane Ni_4Ln_2 (Ln = Gd, Tb, Dy, Ho) and Ni_4Y_2 Complexes: Rare Tb (III) and Ho (III) Examples Showing SMM Behavior. *Inorg. Chem.* **2014**, *53*, 3519−3525.
(45) Zhao, X.-Q.; Lan, Y.; Zhao, B.; Cheng, P.; Anson, C. E.; Powell, A. K. Magnetic quantum tunneling: insights from simple molecule-based magnets. *Dalton Trans.* **2010**, *39*, 4911−4917.
(46) Bag, P.; Chakraborty, A.; Rogez, G.; Chandrasekhar, V. Lanthanide double-decker complexes functioning as magnets at the single-molecular level. *Inorg. Chem.* **2014**, *53*, 6524−6533.
(47) Li, M.; Lan, Y.; Ako, A. M.; Wernsdorfer, W.; Anson, C. E.; Buth, G.; Powell, A. K.; Wang, Z.; Gao, S. A Family of 3d-4f Octa-Nuclear $[Mn^{III}_4Ln^{III}_4]$ Wheels (Ln = Sm, Gd, Tb, Dy, Ho, Er, and Y): Synthesis, Structure and Magnetism. *Inorg. Chem.* **2010**, *49*, 11587−11594.
(48) Chandrasekhar, V.; Pandian, B. M.; Vittal, J. J.; Clerac, R. Synthesis, Structure, and Magnetism of heterobimetallic trinuclear complexes {$[L_2Co_2Ln][X]$} [Ln = Eu, X = Cl; Ln = Tb, Dy, Ho X = NO_3, LH_3=(S)P[N(Me)N═CH-C_6H_3-2-OH-3-Oe]3]: A 3d-4f- Family of Single-Molecule Magnets. *Inorg. Chem.* **2009**, *48*, 1148−1157.
(49) Bencini, A.; Gatteschi, D. *EPR of Exchange Coupled Systems*; Bencini, A.; Gatteschi, D., Eds.; Dover Publications, Inc.: Mineola, New York, 2012.
(50) Andruh, M.; Ramade, I.; Codjovi, E.; Guillou, O.; Kahn, O.; Trombe, J. C. Crystal Structure and Magnetic Properties of $[Ln_2Cu_4]$ Hexanuclear Clusters (where Ln = tivalent lanthanide). Mechanism of the Gd(III)-Cu(II) Magnetic Interaction. *J. Am. Chem. Soc.* **1993**, *115*, 1822−1829.
(51) Ishida, T.; Watanabe, R.; Fujiwara, K.; Okazawa, A.; Kojima, N.; Tanaka, G.; Yoshii, S.; Nojiri, H. Exchange coupling in TbCu and DyCu single-molecule magnets and related lanthanide and vanadium analogs. *Dalton Trans.* **2012**, *41*, 13609−13619.
(52) Bernot, K.; Bogani, L.; Caneschi, A.; Gatteschi, D.; Sessoli, R. A Family of Rare-Earth-Based Single Chain Magnets: Playing with Anisotropy. *J. Am. Chem. Soc.* **2006**, *128*, 7947−7956.
(53) Schmidt, S.; Prodius, D.; Mereacre, V.; Kostakis, G. E.; Powell, A. K. Unprecedented chemical transformation: crystallographic evidence for 1,1,2,2-tetrahydroxyethane captured within an Fe_6Dy_3 single molecule magnet. *Chem. Commun.* **2013**, *49*, 1696−1698.
(54) Peng, Y.; Mereacre, V.; Anson, C. E.; Powell, A. K. Multiple superhyperfine fields in a {$DyFe_2Dy$} coordination cluster revealed using bulk susceptibility and ^{57}Fe Mössbauer studies. *Phys. Chem. Chem. Phys.* **2016**, *18*, 21469−21480.
(55) Ako, A. M.; Waldmann, O.; Mereacre, V.; Klöwer, F.; Hewitt, I. J.; Anson, C. E.; Güdel, H. U.; Powell, A. K. Odd-numbered Fe^{III} complexes: Synthesis, Molecular Structure, Reactivity, and Magnetic Properties. *Inorg. Chem.* **2007**, *46*, 756−766.
(56) Langley, S. K.; Ungur, L.; Chilton, N. F.; Moubaraki, B.; Chibotaru, L. F.; Murray, K. S. Structure, Magnetism and Theory of a Family of Nonanuclear $Cu^{II}_5Ln^{III}_4$-Triethanolamine Clusters Displaying Single-Molecule Magnet Behaviour. *Chem. - Eur. J.* **2011**, *17*, 9209−9218.

DOI: 10.1021/acs.inorgchem.6b02682
Inorg. Chem. 2017, 56, 4796−4806